Wound-healing, antibacterial, and antinociceptive properties of *Salvia rosmarinus* Spenn. leaves, along with *in silico* analysis

Zineb Lakache,[1] Mourad Ounissi,[1,2] Hinda Hacib,[1] Hamza Aliboudhar,[3] Mohcene Sadallah,[1] Affaf Laassami,[4] Hassina Tounsi,[1] Abdelkrim Kameli[1]

[1]Laboratory of Ethnobotany and Natural Substances, ENS-Kouba, Algiers; [2]Faculty of Natural and Life Sciences, University of Djelfa, Djelfa; [3]USTHB, Laboratory of Functional Organic Analysis, Faculty of Chemistry, University of Sciences and Technology Houari Boumediene, El Bab-Ezzouar, Algiers; [4]Microbial Systems Biology Laboratory, LBSM, Algiers, Algeria

Abstract

This research aimed to characterize the key components of the essential oil extracted from *Salvia rosmarinus* Spenn. (formerly *Rosmarinus officinalis* L.) through hydrodistillation and to explore its *in vivo* wound healing, antinociceptive, and antibacterial properties. Notable compounds identified in the essential oil included d-camphor, camphene, α-pinene, and eucalyptol. *In vivo* experiments involved inducing wounds in mice, which were then treated with the essential oil, leading to significantly accelerated wound healing and repair with a topical application success rate of 82.6%. The analgesic activity of the essential oil was evaluated by the acetic acid test in mice: the results indicated that a dose of 400 mg/kg led to 96.24% pain inhibition. The antibacterial properties of *S. rosmarinus* were evaluated using the agar diffusion method, demonstrating strong antibacterial activity against both *Staphylococcus aureus* and *Escherichia coli*, with inhibition zone diameters of 17 mm and 15 mm, respectively. To support the phytochemical analysis, *in silico* studies were made to identify potential compounds from 30 *S. rosmarinus* essential oils that could inhibit significant drug targets such as human cyclooxygenase-2 (hCOX-2), an anti-inflammatory target, and human transient receptor potential vanilloid1 (hTRPV1), a highly sought-after pain therapy target. These identifications were conducted using molecular docking and molecular dynamics simulation methods. Overall, this study supports the therapeutic use of *S. rosmarinus* for pain prevention and wound healing, underscoring its potential for developing clinically valuable products.

Correspondence: Zineb Lakache, Laboratory of Ethnobotany and Natural Substances, ENS-Kouba, Algiers.
E-mail:lakache.zineb@gmail.com

Key words: excision wound, incision wound, *in silico*, GC/MS.

Contributions: all authors contributed significantly to this work, including drafting and revising the manuscript.

Conflict of interests: the authors declare no conflict of interest.

Ethics approval: all the experiments were carried out according to the guidelines of the Institutional Animal Care Committee of the Algerian Higher Education and Scientific Research (Agreement Number 45/DGLPAG/DVA.SDA.14).

Availability of data and materials: all data generated or analyzed during this study are included in this published article.

Informed consent: not applicable.

Received: 3 July 2024.
Accepted: 17 March 2025.
Early view: 17 July 2025.

Journal of Biological Research 2025; 98:12778
doi:10.4081/jbr.2025.12778

Introduction

Phytotherapy, in its classical interpretation, refers to the medical field that employs whole plants or their components for medicinal purposes, aiming to treat or prevent a diverse array of diseases. Rooted in numerous medical traditions throughout history, particularly in Ayurvedic medicine, traditional Chinese medicine, and naturopathic medicine,[1] plant-derived products have consistently served as the bedrock for addressing various health conditions. This reliance on plant-based remedies spans centuries, leveraging traditional wisdom concerning the therapeutic attributes of specific plants and their active molecules.[2]

The cicatrization process, an inherent aspect of wound recovery applicable across various causative factors, is a systemic and dynamic phenomenon intricately connected to the overall health conditions of the organism.[3] Wound healing unfolds as a meticulously orchestrated sequence of cellular, molecular, and biochemical events working in concert to achieve tissue restoration. The critical components include inflammation, cell proliferation, the development of granulation tissue, wound contraction, and the subsequent remodeling phase.[4-6] As phytotherapy earns greater recognition as a scientific field, [6-9] there is a growing need to establish comprehensive guidelines that will enhance our understanding of its clinical applications, effectiveness, and safety.[9] In the extensive exploration of various plants and their active com-

ponents in this emerging field, the rosemary plant, *Salvia rosmarinus* Spenn. (previously known as *Rosmarinus officinalis* L.), stands out as an aromatic and medicinal herb widely distributed in the Mediterranean region. Rosemary, a well-known shrub with a distinctive strong aroma, belongs to the Lamiaceae family.[10] The growing recognition of its clinical utility[11] is further supported by advancements in innovative methods for the targeted extraction of its bioactive metabolites.[12]

Research on the analgesic, antioxidant, and wound-healing effects of the essential oil from *S. rosmarinus* has gained attention in recent years, with several studies highlighting its potential biological properties, including its role in promoting wound healing. However, despite these findings, the specific mechanisms underlying these effects, particularly the contribution of key bioactive compounds within the essential oil, remain unclear. To address this gap, the present study not only aims to evaluate the healing effect of the essential oil obtained from the leaves of *S. rosmarinus* on cutaneous lesions induced in mice, but also to provide insight into its mechanism of action through an *in silico* approach. By employing a virtual screening workflow and molecular dynamics simulation, we identified potential key compounds with anti-inflammatory and analgesic properties, offering a deeper understanding of how the essential oil contributes to its therapeutic effects.

Materials and Methods

Plant material

Leaves of *S. rosmarinus* were gathered in February 2023 from the El-Bayadh region in Southwest Algeria, specifically located at Latitude: 33° 40′ 49″ N; Longitude: 1° 01′ 13″ E; Altitude: 1,313 m. Professor Toumi from the Department of Biological and Environmental Sciences at ENS Kouba, Algeria, identified the plant. These plant samples are now stored at the Institute of Science at the University of El-Bayadh, Algeria, under the reference number CA99/11. The harvested plant parts were naturally air-dried in a shaded area at ambient temperature.

Hydrodistillation extraction

The essential oil of *S. rosmarinus* was acquired through hydrodistillation employing the Clevenger method. The plant material was combined with water in a flask and allowed to sit for two hours. Subsequently, the obtained oil was separated from the water using a straightforward decantation process, without the incorporation of any organic solvents. The extracted oil was then preserved in a tightly sealed brown vial, stored in a dark and cool place at 4°C.

Gas Chromatography/Mass Spectrometry (GC/MS)

The essential oil of *S. rosmarinus* underwent chemical analysis through Gas Chromatography-Mass Spectrometry (GC/MS) utilizing a Gas Chromatography-Mass Spectrometry Flame Ionization Detector (GC-FID) system 7890A/5977B Mass Selective Detector (MSD) (Agilent Technologies, Wilmington, DE, USA). A fused-silica-capillary column with a non-polar stationary phase HP5MS (30 m×0.25 mm×0.25 µm film thickness) was employed in the analysis. The GC procedure involved injecting a volume of 0.2 µL into the splitless GC inlet, maintained at 250°C. The column temperature program included an initial period at 60°C for 8 minutes, followed by a gradual increase at a rate of 4°C/minute to reach 250°C, which was then maintained for 25 minutes. The ionization mode utilized was electronic impact at 70 eV.

The identification of the chemical constituents was accomplished by comparing the mass spectral fragmentation patterns with those stored in databases such as Adams 2017, NIST 2014, and Wiley. Additionally, the retention indices of the volatile extract constituents were compared with published index data for further confirmation.

Experimental animals

A total of 24 Swiss albino mice, weighing between 20-25 g, were obtained from the Pasteur Institute in Algiers. Mice were accommodated in standard cages under controlled environmental conditions, maintaining a temperature of 25±1°C and a 12-12 hours light-dark cycle. Following their acquisition, the mice were allowed a week for acclimatization to the laboratory conditions. During this period, they had unrestricted access to both water and a standard pellet diet. All experimental protocols adhered to the guidelines established by the Institutional Animal Care Committee of Algerian Higher Education and Scientific Research. This compliance was documented by Agreement Number 45/DGLPAG/ DVA.SDA.14.

Preparation of topical formulations

A combination of 7 g of beeswax and 14 mL of soya oil was subjected to heating using a bain-marie method, resulting in a liquid mixture or cream. The cream, comprised of beeswax and soya oil, served as the base to which essential oil was added until reaching a concentration of 8% (v/w). Subsequently, the topical formulations were meticulously packaged, labeled, and stored at 4°C until required for use.

The decision to use an 8% concentration of *S. rosmarinus* essential oil cream in our study was informed by previous *in vitro* investigations, which demonstrated its effectiveness in promoting wound healing and providing analgesic benefits. Based on these promising outcomes, we selected this concentration as the optimal dosage for our research.

Wound healing studies

Excision wound model

The mice involved in this study were initially anesthetized intraperitoneally with ketamine (100 mg/kg) and xylazine (10 mg/kg) to induce anesthesia for the creation of wounds. The dorsal region of each mouse was shaved, and four wounds were generated using a 5 mm punch, spaced approximately 1 cm apart. Post-surgery, the mice were individually housed to prevent any interference with the natural wound-healing process.[13] A total of 24 mice were randomly distributed into three groups, each consisting of eight mice. Group I served as the control with no treatment, Group II received a commercial ointment (Madecassol® cream, Bayer Healthcare SAS, France), Group III was treated with a 8% essential oil cream of *S. rosmarinus*.

Throughout a 10-day period, all mice underwent daily topical treatment using sterile swabs. The evaluation of wound healing was conducted by measuring wound closure during this timeframe. The assessment of wound closure was performed using ImageJ software, and the percentage of wound closure was calculated using the following formula:

$$\text{Percentage of wound closure} = \frac{(\text{Initial wound area} - \text{Current wound area}) \times 100}{\text{Initial wound area}}$$

Incision wound model

All animals were anaesthetized with ketamine (100 mg/kg) and xylazine (10 mg/kg) and the back hairs of mice were shaved by using a shaving machine. Three cm long, linear paravertebral incisions were made with a sterile surgical blade through the full thickness of the skin at the distance of 1.5 cm from the midline of each side of the vertebral column.[14] The wounds were closed with tow surgical interrupted sutures of 1 cm apart. The animals were divided into three groups. Group I served as the control and received no treatment, while Group II received a commercial ointment of Madecassol® cream and Group III received the 8% essential oil cream of *S. rosmarinus*. The sutures were taken out on day 9 following the incision, and the therapy continued until day 10. The degree of healing was subsequently evaluated by measuring the tensile strength (TS) on the tenth day.

$$\%\ \text{Tensile strength of extract} = \frac{(\text{TS extract} - \text{TS vehicle}) \times 100}{\text{Ts vehicle}}$$

Antibacterial Activity

Different bacterial strains (*Escherichia coli* and *Staphylococcus aureus)* were inoculated on Mueller-Hinton agar. After 24 hours of incubation at 37°C, a microbial suspension was prepared with physiological water (NaCl 0.9%), diluted, and adjusted to a concentration of 0.5 McFarland. Mueller-Hinton agar, the selected medium, was poured into 90 mm diameter Petri dishes and inoculated with a freshly prepared pure microbial suspension.

Sterile Whatman filter paper discs, 6 millimeters in diameter, were impregnated with 10 µL of essential oil at a concentration of 100 mg/mL and aseptically placed on the inoculated agar.

The entire set was incubated for 24 hours at 37°C for evaluating bacteria growth. The zones of inhibition around the 6 mm discs were then observed and measured.

Acute toxicity

The acute toxicity of *Salvia rosmarinus* essential oil was evaluated by testing various carefully selected doses of the oil. All doses were diluted in a physiological saline solution (0.9% NaCl).[11] The study involved four groups, each comprising six mice, with oral administration conducted through a gastric tube. The control group received only the physiological saline solution orally. The remaining groups were orally administered with different doses of the essential oil (at 400, 600, and 1000 mg/kg). Following administration, the mice were closely observed for 72 hours to monitor signs of toxicity and evaluate the mortality rate.

Antinociceptive activity

The analgesic activity of the essential oil of *S. rosmarinus* was assessed using the method described by Collier *et al*.[15] The evaluation involved the observation of the ability of the analgesic substance to reduce movements in mice. The study included four groups, each comprising six mice, with different doses administered orally using a gastric tube. The doses were as follows: a control group receiving a physiological water solution (0.9%), a reference group receiving an acetyl salicylic acid (aspirin®) solution at a concentration of 100 mg/kg, and two treated groups receiving essential oil at doses of 200 mg/kg and 400 mg/kg, respectively.

One hour after oral administration, each mouse received an intraperitoneal injection of 0.2 mL of a 3% acetic acid solution. The number of writhings for each mouse was then counted ten minutes after injection, and observed over a total duration of ten minutes. The percentage reduction of pain was calculated using the following formula:

$$\%\ \text{Reduction of pain} = \frac{(\Delta T - \Delta E) \times 100}{\Delta T}$$

Where, ΔT represents the mean number of writhings in the control group treated with physiological water 0.9% NaCl, while ΔE represents the mean number of writhings in the test group treated with the essential oil or positive control.

In-silico studies

To understand the anti-inflammatory and analgesic activity of compounds within essential oils of *S. rosmarinus*, virtual screening via molecular docking and molecular dynamics simulation was conducted. The crystal structures of human Cyclooxygenase-2 (COX-2) complexed with Tolfenamic acid, a non-steroidal anti-inflammatory drug (NSAID) that inhibits COX-2 to reduce pain and inflammation, and human Transient Receptor Potential Vanilloid 1 (hTRPV1) complexed with SmithKline Beecham-366791 (SB-366791), a selective antagonist that blocks hTRPV1 activation to alleviate nociception and inflammatory pain, were obtained from the Protein Data Bank (PDB). These structures are crucial for exploring the molecular mechanisms of inflammation and pain, providing insights into potential therapeutic targets and their interactions with inhibitory compounds. Virtual screening utilized PyRx/AutodockVina on the Linux platform, with protein structures prepared using MGLTOOLS software. The missing P-loop in the hTRPV1 structure was modeled using the ModLoop program. Thirty compounds from *S. rosmarinus*. essential oils were prepared using the Ace Prep tool of the Accellera Playmolecule platform and saved in a single Structure Data File (SDF).

Loop modeling validation

The pore loop model was validated through multiple steps. Firstly, validation was achieved using Ramachandran Plot predicted from Swiss-model[16]. Subsequently, further validation was conducted using the ProSA integrated webserver.[16] This involved assessing the deviation of Z-scores from high-resolution structures and determining potential errors within the model. Additionally, it entailed generating an energy plot that shows the local model quality by plotting energies as a function of amino acid sequence position.[17]

Virtual screening workflow

Grid generation

In molecular docking, grid generation relied on the native co-crystallized inhibitor specific to each structure. Residues with rotatable groups like hydroxyl and thiol around the ligands were then selected. For human cyclooxygenase-2, the grid was generated based on the position of the co-crystallized Tolfenamic acid inhibitor with coordinates 165.45 (x), 185.78 (y), and 192.26 (z). For hTRPV1, the grid was based on the position of the analgesic drug SB-366791 with coordinates 105.40 (x), 80.96 (y), and 88.40 (z).

Virtual screening

In order to find and effectively rank the natural compounds in the binding sites of the target protein structures, 30 natural compounds of *S. rosmarinus*. essential oils were screened using PyRx/AutodockVina. The detection of binding sites within the uti-

lized protein structures was conducted through gride sites. The optimal compound pose, which refers to the most favorable spatial orientation and arrangement of a compound within the protein's binding site, was selected based on its docking score. This configuration is retained for detailed interaction analyses and to predict the potential biological activity of the compound. The binding poses of screened compounds within the binding site were subsequently ranked based on their binding affinity (docking score) for protein-ligand complexes, reported in kcal/mol.

Molecular dynamics simulation

To verify the stability of all the complexes generated in the docking and binding analyses, a molecular dynamics (MD) simulation lasting 200 nanoseconds was performed. This computational technique models the physical movements of atoms and molecules over time to evaluate how stable the interactions are within each protein-ligand complex in a dynamic and realistic biological environment. By observing these complexes during the simulation, critical information about their structural stability, conformational changes, and the persistence of specific interactions (e.g., hydrogen bonds or hydrophobic contacts) can be gained. This process helps predict whether a ligand could maintain its binding affinity under physiological conditions.

System building

Anti-inflammation and pain

System 01: the complex of the human Cyclooxygenase-2 (hCOX-2) with the natural compound; Alpha calacorene (5IKT/ Alpha-calacorene).

System 02: the complex of the Human Transient receptor potential vanilloid 1 (hTRPV1) with the natural compound Beta_Bisabolene (8GFA/ Beta_Bisabolene).

The TIP3P model, short for Transferable Intermolecular Potential with 3 Points, is a simplified but effective representation of water molecules frequently used in molecular dynamics simulations. It treats water as consisting of three interaction points: one for oxygen and two for hydrogens, with specific charges and interaction parameters assigned to approximate water's physical and chemical behaviors, such as hydrogen bonding and dipole interactions. In this context, the two studied systems were solvated using the TIP3P water model, meaning they were embedded in a simulated aqueous environment for molecular stability. These simulations occurred in an orthorhombic box with 1 nm dimensions on each side, using a buffer calculation method to ensure accurate interactions with the surroundings. This setup allows the molecules to behave as they would in water, helping validate system stability and dynamics. To maintain system neutrality, Na^+ ions were introduced. Additionally, a combination of Na^+ and Cl^- ions was incorporated to achieve a concentration of 150 mM, simulating the physiological conditions.

Molecular dynamics setup

The molecular dynamics (MD) simulation described uses DESMOND V7.2, a high-performance simulation software designed for studying large biomolecular systems, coupled with the OPLS2005 force field, which governs the interactions between atoms during simulations. The simulation was run on a Linux system with Graphics Processing Units (GPU) acceleration, utilizing GPU to speed up the calculation-intensive process, crucial for handling large systems and extended simulation times. The simulation employed the NPγT ensemble (normal pressure, constant surface tension, and temperature) for membrane proteins, and the NPT ensemble (normal pressure and temperature) for other complexes. This approach ensures the correct physical conditions are applied, such as maintaining constant pressure and temperature. The system underwent 300 nanoseconds (ns) of MD simulation, with sampling intervals of 1.2 ps for energy and 30 ps for trajectory data. These sampling intervals ensure the system is analyzed at sufficient intervals, capturing essential dynamic behaviors, while a 100 ps minimization step and subsequent relaxation are employed to avoid steric clashes and stabilize the system before running the full simulation.

Statistical analysis

The mean values of the data were reported alongside the standard deviation (SD). Statistical analysis was conducted through a one-way analysis of variance (ANOVA) test, followed by the Tukey test to identify significant differences between groups (*$p<0.05$, **$p<0.01$, and ***$p<0.001$).

Results

Hydrodistillation extraction

The essential oil extracted from the leaves of *S. rosmarinus* using hydrodistillation exhibited a green-yellowish color and yielded 2.39%.

Gas Chromatography/Mass Spectrometry (GC/MS)

The findings revealed the presence of 30 components, constituting 98.82% of the total oil. These components have been identified, and their retention indices along with relative area percentages are outlined in Table 1. The essential oil exhibited a significant concentration of the major compound, d-camphor (37.84%), followed by camphene (14.36%), α-pinene (11.15%), eucalyptol (9.2%), limonene (4.12%), o-cymene (3.93%), borneol (2.88%), α-bisabolol (2.58%), α-terpineol (2.25%), 4-terpineol (1.36%), and bornyl acetate, caryophyllene, τ-muurolene, τ-cadinene, copaene, tricyclene, each present in amounts less than 1% of the essential oil.

In this GC-MS analysis, the majority of compounds were clearly identified and quantified, accounting for 98.8% of the total. The remaining 1.2% represents a negligible proportion compared to the identified compounds. This discrepancy can be attributed to the detection and quantification limits of the instrument. Some compounds may be present at extremely low concentrations, making their identification challenging due to background noise and sensitivity constraints. Consequently, small peaks observed on the chromatogram, often near the detection threshold, correspond to these 1.2% of unidentified compounds**,** whose low intensity prevents reliable identification.

Wound healing evaluation

Excision wound

The advancement of wound healing can be assessed by measuring wound closure, representing the percentage reduction in the wound area over time. In this investigation, wound healing progress was compared across experimental groups during a 10-day treatment period, as depicted in *Figure 1S*. On the 6th day, Groups II (treated with Madecassol® cream) and III (treated with 8% *S. rosmarinus* cream) exhibited significantly higher percentages of wound closure

($p<0.001$) than Group I (control). Wounds treated with *S. rosmarinus* showed accelerated closure after 8 days of treatment (Figure 1 and *Figure 1S*). By the 10th day, wounds treated with 8% *S. rosmarinus* cream demonstrated a greater percentage of wound closure (82.6%) compared to the control group (42.64%).

Incision wounds

Despite complete healing of all incised and sutured wounds (*Figure 2S*), the recorded tensile strengths varied. According to Table 2, both the standard medication (Madecassol®) and the *S. rosmarinus* cream-treated groups exhibited increases in breaking strength of 68.25% and 76.58%, respectively.

Antibacterial activity

We assessed the antibacterial properties of *S. rosmarinus* essential oil using the agar diffusion method. The oil's effectiveness was tested against two bacterial strains: *Escherichia coli* and *Staphylococcus aureus*. According to our results, *S. rosmarinus* essential oil demonstrated strong antibacterial activity against both *Staphylococcus aureus* and *Escherichia coli*, with inhibition zone diameters of 17 mm and 15 mm, respectively.

Acute toxicity

The results revealed that the essential oil of *S. rosmarinus* did not induce any signs of toxicity or mortality in mice across various trials, even when orally administered at a dose of 1,000 mg/kg.

Antinociceptive activity

In this investigation, pain was induced in mice through intraperitoneal injections of acetic acid. Our results demonstrated that the administration of *S. rosmarinus* essential oil at a dose of 400 mg/kg led to a higher writhing inhibition percentage of 96.24%, in contrast to the lower dose of 200 mg/kg, which exhibited a writhing inhibition percentage of 78.95% (*Figure 3S*, Table 3).

Table 1. Chemical composition of the *S. rosmarinus* essential oil.

N°	RT[a]	Compound[b]	RI[c]	RI[d]	% Peak area
1	4.620	Tricyclene	912	914	0.511
2	5.045	α-Pinene	923	930	11.158
3	5.501	Camphene	934	934	14.362
4	6.560	β-Pinene	960	964	0.348
5	7.313	β-Myrcene	978	980	0.383
6	7.950	α-Thujene	994	996	0.152
7	8.596	α-Terpinene	1008	1008	0.310
8	9.045	o-Cymene	1018	1018	3.935
9	9.289	Limonene	1023	1022	4.122
10	9.383	Eucalyptol	1025	1026	9.252
11	13.482	Fenchol	1110	1111	0.259
12	14.893	d-Camphor	1140	1144	37.837
13	15.744	Borneol	1159	1159	2.889
14	16.249	4-Terpineol	1169	1171	1.364
15	16.848	α-Terpineol	1182	1182	2.256
16	20.524	Bornylacetate	1281	1282	0.846
17	23.487	Ylangene	1368	1368	0.132
18	23.642	Copaene	1372	1371	0.531
19	25.049	Caryophyllene	1414	1416	0.869
20	26.141	α-Caryophyllene	1449	1449	0.223
21	26.927	τ-Muurolene	1473	1473,3	0.676
22	27.167	α-Curcumene	1481	1481	0.223
23	27.672	α-Muurolene	1497	1494,6	0.318
24	27.972	β-Bisabolene	1508	1507	0.236
25	28.076	τ-Cadinene	1511	1512	0.644
26	28.380	δ-Cadinene	1523	1523	1.540
27	28.927	α-Calacorene	1544	1544	0.242
28	30.075	Caryophylleneoxide	1587	1585	0.368
29	31.779	τ-Cadinol	1644	1643	0.252
30	33.039	α-Bisabolol	1685	1684	2.585
				Total	98.823

[a]Compounds identified according to their families on HP-5MS column; [b]retention indices with respect to C5–C28 n-alkanes calculated on non-polar HP5-MS capillary column; [c]retention indices given in the literature (NIST, Wiley or ADAMS on non-polar HP-MS or DB5-MS capillary column); [d]percentage calculated from the peak areas of GC chromatogram on non-polar HP5-MS capillary column. RI, retention indices; RT, retention time.

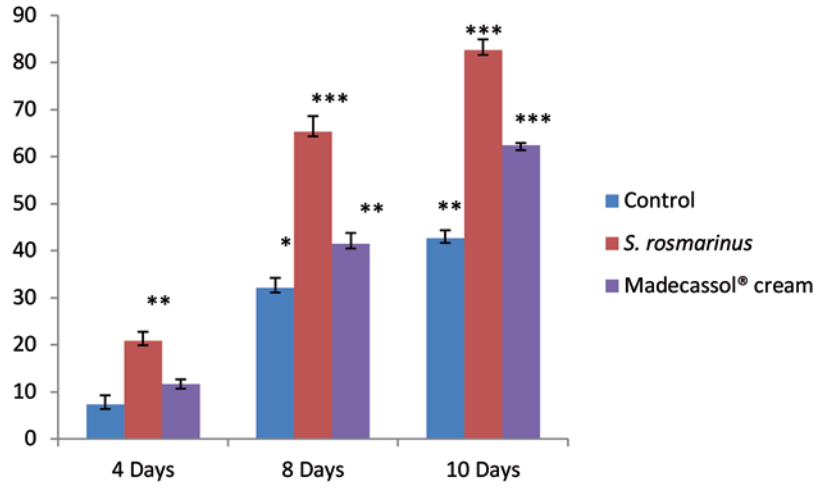

Figure 1. Percentage of wound closure in experimental groups during the treatment days of essential oil cream of *S. rosmarinus*, Madecassol® cream and control of excision wound model in mice.*$p < 0.05$, **$p < 0.01$, and ** $p < 0.001$ are considered significant, compared to the control.

Pore loop modeling

Both the Ramachandran plot (*Figure 4Sf*) and the Z-score, along with associated energy plot statistics (*Figure 4Se*), were acquired from the Swiss model and ProSA web servers, respectively. The Ramachandran plot statistics implies that the modeled 3D structure of the Pore loop of hTRPV1 has its residues in the most favored and allowed regions, validating the quality of the modeled 3D structure.

The figure depicts the location of the Z-score for the structure of hTRPV1 and the pore loop. The values, -7.58 and -1.01 for the subunit of hTRPV1 and the pore loop, respectively, fall within the range of native conformations. Additionally, the residual energies of the P-loop are largely negative, as depicted in the figure.

Virtual screening using Docking

Cyclooxygenase-2

The virtual screening against COX-2 as the anti-inflammatory target, identified α-calacorene as the sole compound binding to its binding pocket, exhibiting a notable free binding affinity of -8.00, and establishing hydrophobic interactions within a cutoff distance of 0.3 nm (Figure 2). The Figure 2a shows that the conformation of α-calacorene exhibited a pose similar to that of Tolfenamic acid.

Transient receptor potential vanilloid 1 (hTRPV1)

The virtual screening analysis against the hTRPV1, the most sought-after pain therapy targets,[18] has unveiled that *β*-bisabolene stands out as the sole compound within *S. rosmarinus* essential oils capable of binding to the Vanilloid pocket of the hTRPV1 (Figure 3), exhibiting a binding affinity of -6.3 kcal/mol (*Table 1S*).

Molecular dynamic simulation analysis

Structural stability of the complexes

Molecular dynamic simulations were carried out to evaluate the inhibition efficiency and analyze the interaction of compounds screened from essential oils of *S. rosmarinus*, as well as to evaluate

Table 2. Effect of topical application of cream of *S. rosmarinus* and Madecassol® cream on incision wound model in mice.

Group	Tensile strength (g)	% Tensile strength
Control	252±17.32	-
S. rosmarinus cream	445±15.7**	76.58
Madecassol® cream	424±19.46**	68.25

*p <0.05, **p <0.01, and ***p <0.001 are considered significant, compared to the control.

Table 3. Percentage of inhibition of abdominal contractions induced by acetic acid in mice.

Treatment	Dose (mg/kg)	% Inhibition
Aspirin®	100	68.53
S. rosmarinus	200	78.95
S. rosmarinus	400	96.24

the stability within the complexes. Consequently, MD simulations were executed for two specific complexes: hCOX-2 with α-calacorene and hTRPV1 with β-bisabolene.

The stability and convergence of the molecular simulation for both system complexes were verified through the plotting of the root-mean-square deviation (RMSD) of the backbone Cα and the heavy atoms of the ligands, along with the root mean square fluctuation (RMSF), across a timescale ranging from 0 to 300 ns for each complex.

RMSD analysis

In the *Figure 5Sa*, the RMSD values of the protein backbone Cα and the ligand for each step versus time are depicted for the hCOX-2/α-calacorene complex. It is observed that the complex reached equilibrium at approximately 75 ns.

Furthermore, it demonstrates the stability of the compound α-calacorene within the protein's binding site compared to its reference conformations. The plot of the calculated RMSD values indicates that the compound is anchored within the binding site of the hCOX-2, exhibiting remarkable long-term stability. The RMSD values were ranging from 0.025 nm to 0.075 nm (*Figure 5Sa*).

Additionally, the *Figure 5Sb* displays a structural superposition of 41 conformations obtained from the simulation trajectory, relative to their initial conformation, with intervals of 250 frames (equivalent to 7.47ns). This superposition illustrates the absence of significant structural changes in the complex, indicating that all ligands persist within their respective binding sites.

On the other hand, the hTRPV1 and β-bisabolene complex reach equilibrium at 50 ns, as depicted in *Figure 6Sb*, and maintain stability throughout the simulation trajectory. Furthermore, the RMSD plots for β-bisabolene compound exhibit consistent conformational stability with internal mobility. The RMSD values range between 0.01 nm to 0.09 nm along the simulation trajectory (*Figure 6Sb*).

Moreover, the *Figure 6Sa* illustrates a structural superposition of 41 conformations of the complex, each separated by an interval of 250 frames (equivalent to 7.47ns). This analysis discerns that throughout the simulation trajectory no notable structural alterations occurred within the complexes, indicating the ligands persistently occupying their respective binding sites.

RMSF analysis

The root mean square fluctuation (RMSF) is a valuable metric for characterizing local conformational changes along the protein chain. By quantifying the fluctuations in atomic positions, the RMSF provides insights into the flexibility of different regions of the protein. Notably, the RMSF can be directly correlated with experimental B-factors, which are typically used to represent the atomic displacement or mobility in X-ray crystallography. Ideally, the RMSF values should show a parallel trend with the experimentally measured B-factors reported in the Protein Data Bank (PDB) files, offering a reliable comparison between computational and experimental data.

For the complex hCOX-2/α-calacorene, the RMSF plot shown in *Figure 5Sc* illustrates the root-mean-square fluctuation (RMSF) values calculated for the hCOX-2 Cα atoms throughout the simulation period. In this figure, the RMSF curves reveal only minor differences in the flexibility of the hCOX-2 states, confirming the absence of significant conformational changes during the simulations. Overall, notable conformational flexibility was observed in loop regions compared to secondary structural elements such as alpha helices and beta strands, which typically exhibit greater rigidity.

For complex hTRPV1/β-bisabolene the RMSF plot in the *Figure 6Sc* shows that the high fluctuations of residues were particularly found in the Pore loop and the tails (N- and C-terminal) regions, with regard to secondary structure elements like alpha helices and beta strands are usually more rigid.

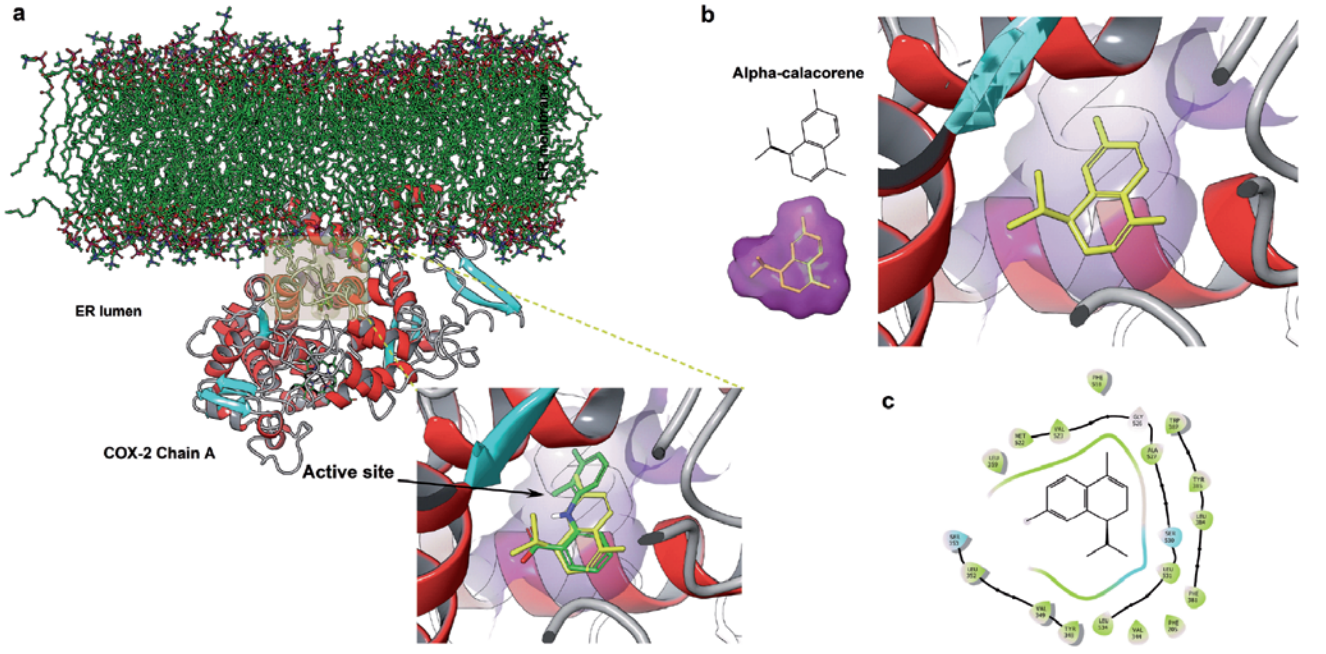

Figure 2. Binding mode of the screened natural compound α-calacorene and the co-crystallized Tolfenamic acid within the binding site of human Cyclooxygenase-2: (a) superimposition of α-calacorene and Tolfenamic acid represented in yellow and green, respectively; (b) the hydrophobic pocket is depicted in purple, occupied by α-calacorene; (c) COX-2, Cyclooxygenase-2; ER, Endoplasmic Reticulum.

On the other hand, *Figures 5Sc* and 6Sc represent a comparison of the temperature B-factor with the RMSF values derived from the MD simulation of the two complexes. It is noticeable that the experimental B-factors of two complexes significantly correlate with RMSFs.

Discussion

Our results indicated that the essential oil extracted from the aerial parts of *S. rosmarinus* yielded 2.39%. In a recent study by Elyemni *et al.*,[19] the yield of *R. officinalis* (former name of *S. rosmarinus*) essential oil was reported to be 1.35±0.04% for cultivated plants from the Fez region, Morocco, and 2.24±0.05% for wild *R. officinalis* from the Figuig province, Morocco. This difference in extraction yields can be attributed to various factors, including the degree of plant maturity, climate conditions, soil composition, harvesting time, extraction method, and the geographical position of the plant species.[20]

However, it is crucial to acknowledge that the chemical composition and antioxidant activity of the essential oil can be affected by several factors. One of such factor is the extraction method, such as hydrodistillation, which has the potential to cause the degradation of bioactive compounds. During hydrodistillation, thermal degradation, hydrolysis, and solubilization of bioactive compounds in water may take place, resulting in alterations of their antioxidant capacity. Moreover, the presence of water in hydrodistillation can render several antioxidants unstable or make them susceptible to enzymatic degradation within the moist plant material.[21]

Concerning the suggested mechanisms of action for wound healing attributed to various monoterpenes, these include antimicrobial activity, which hinders the RNA and protein biosynthesis of microorganisms. Additionally, they exhibit anti-inflammatory effects by reducing the production of Interleukin (IL)-6 and Tumor Necrosis Factor (TNF)-α in mast cells, inhibiting the release of leukotriene C4 (LTC4), and influencing the release of thromboxane B2 (TxB2). Furthermore, monoterpenes possess antioxidant properties, delivering photoprotective effects and inhibiting the generation of free radicals induced by Ultraviolet B (UVB) radiation. Notably, they demonstrate low toxicity and impact macrophage migration inhibitory factors and fibroblast growth.[22]

Other research showed that *S. rosmarinus* is rich in phenolic compounds and exhibits noteworthy anti-inflammatory capacity, as documented in previous studies.[9,12] This anti-inflammatory potential is closely linked to its observed wound healing properties. The wound healing activity observed in this study can be ascribed to the elevated percentages of key components, specifically camphor, camphene, α-pinene, and 1,8-cineole, all of which

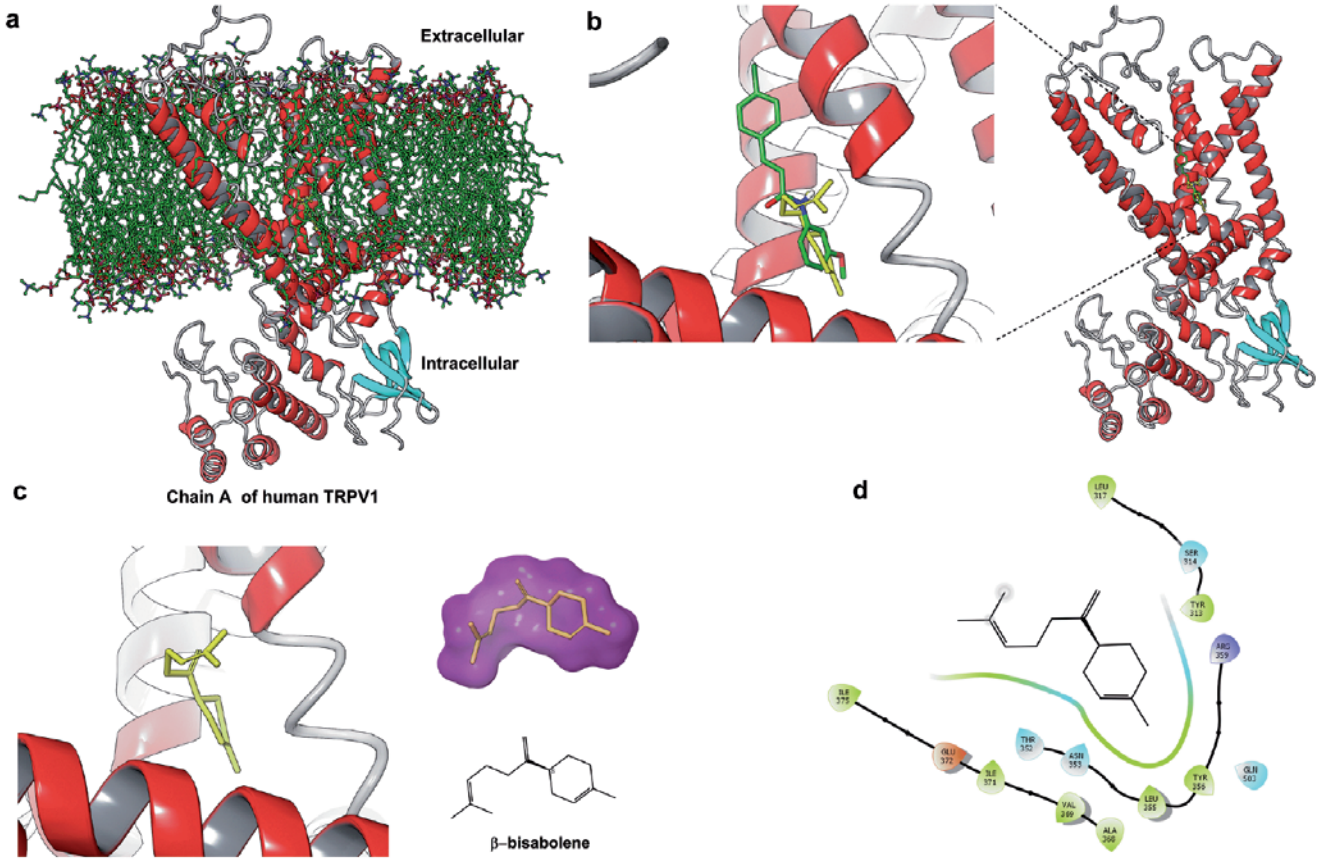

Figure 3. Structural details illustrating the binding mode of the screened natural compound β-bisabolene and the co-crystallized inhibitor SB-366791 within the Vanilloid pocket of human hTRPV1; (a) subunit A of hTRPV1 embedded in the interior of lipid bilayers of cell membrane; (b) superposition of β-bisabolene and the SB-366791 inhibitor shown in yellow and green, respectively; (c) the compound β-bisabolene within the Vanilloid pocket; (d) 2D ligand interaction diagram of β-bisabolene within the Vanilloid pocket interacting via hydrophobic contacts. hTRPV1, human transient receptor potential vanilloid1.

have been associated with wound-healing properties. Moreover, terpenes like pinene, limonene, and sabinene, recognized for their antioxidant properties, may contribute to the observed wound healing activity, even though they constitute a relatively lower percentage of our essential oil.[23]

Acute inflammation plays a critical role in the early stages of wound healing by producing essential factors such as cytokines. This inflammatory phase is crucial for eliminating microorganisms like *Staphylococcus aureus* and *Pseudomonas aeruginosa*. However, incomplete removal of these microorganisms can delay the healing process and damage the extracellular matrix. It has been demonstrated that inhibiting wound remodeling and matrix synthesis can significantly hinder wound closure. Previous studies have confirmed the antibacterial activity of *Rosmarinus officinalis*, attributed to compounds such as 1,8-Cineole and α-Pinene, particularly effective against *Pseudomonas aeruginosa* and *Staphylococcus aureus*.[24] Our results showed that a cream containing *S. rosmarinus* significantly reduced bacterial growth and colonization in treated animals, likely due to its antibacterial properties. Additionally, 1,8-Cineole has been reported to inhibit the production of pro-inflammatory cytokines, which are associated with tissue inflammation in various wounds, including diabetic wounds. Consequently, 1,8-Cineole is suggested to possess both anti-inflammatory and antibacterial properties.

Our findings demonstrate that the essential oil derived from *S. rosmarinus* did not display any signs of toxicity or cause mortality in mice across a range of tested doses. Supporting this, recent research reported that *R. officinalis* essential oil showed no adverse effects, including in tests conducted on Wistar rats. Notably, even at doses up to 2,000 mg/kg, no toxicity symptoms were observed, underscoring the oil's safety profile.[25]

The intraperitoneal injection of acetic acid induces tissue damage, leading to the release of various chemical mediators such as bradykinin, histamine, serotonin, acetylcholine, and prostaglandins. Prostaglandins, in particular, sensitize nociceptors to painful stimuli, resulting in consequent widespread pain. In mice, this pain is manifested through the stretching of hind limbs and twisting of dorsoabdominal musculature. The essential oil of *R. officinalis* demonstrated a concentration-dependent inhibition of abdominal contractions, suggesting its potential analgesic effect. This observed effect may be attributed to the suppression of chemical mediator release.[26]

To support previous results, molecular docking followed by molecular dynamics simulations were employed to predict the interactions between screened compounds and the binding sites of their protein targets, and to evaluate the strength of these interactions. These critical analyses help investigate the potential of specific compounds, among the 30 identified in *S. rosmarinus*. essential oils, to effectively bind to particular therapeutic targets.

The virtual screening targeting COX-2 for its anti-inflammatory properties identified α-calacorene as the sole compound effectively binding to the enzyme's binding pocket. It demonstrated a significant free binding affinity of -8.00 and established hydrophobic interactions within a 0.3 nm cutoff distance. This finding, along with the previously discussed experimental evidence of anti-inflammatory effects, strongly supports the assertion that α-calacorene is responsible for eliciting an anti-inflammatory response. This conclusion aligns with the observations made by Zaman *et al*.[27]

The virtual screening analysis targeting hTRPV1, one of the most sought-after pain therapy targets,[18] has revealed that β-bisabolene is the only compound within *S. rosmarinus* essential oils capable of binding to the vanilloid pocket of hTRPV1, exhibiting a binding affinity of -6.3 kcal/mol. This interaction suggests its potential role as an allosteric hTRPV1 inhibitor, functioning as an analgesic antagonist. These findings are consistent with the research published by Júnior *et al*. [28]

The Root Mean Square Fluctuation (RMSF) is a useful metric for characterizing local conformational changes along a protein chain. The RMSF values can be correlated with experimental B-factors, which are reported in PDB files. For the hCOX-2/α-calacorene complex, the RMSF plot shown in *Figure 5Sc* illustrates the RMSF values calculated for the hCOX-2 Cα atoms throughout the simulation period. The RMSF curves reveal only minor differences in the flexibility of the hCOX-2 states, confirming the absence of significant conformational changes during the simulations. Overall, notable conformational flexibility was observed in loop regions compared to secondary structural elements such as alpha helices and beta strands, which typically exhibit greater rigidity.

Conclusions

The essential oil of *S. rosmarinus* has shown considerable therapeutic potential, particularly in its analgesic, wound-healing, and antibacterial effects. The oil demonstrated significant pain-reducing properties, attributed to bioactive components such as 1,8-cineole and α-pinene, marking its potential as a natural analgesic. In wound healing, formulations containing rosemary essential oil accelerated the repair of superficial wounds, highlighting its role in promoting tissue regeneration. Moreover, its antibacterial activity proved effective, especially against *Staphylococcus aureus*, which positions it as a promising natural antimicrobial agent. While the oil's safety profile reinforces its suitability for various applications, it is more accurately considered a prerequisite for therapeutic use rather than a therapeutic property in itself. This comprehensive efficacy underscores rosemary essential oil's value as a natural remedy across multiple health domains.

References

1. Falzon CC, Balabanova A. Phytotherapy: An introduction to herbal medicine. Prim Care Clin Off Pract 2017;44:217-27.
2. Piriz MA, Lima CAB, Jardim VMR, et al. Plantas medicinais no processo de cicatrização de feridas: uma revisão de literature [Medicinal plants for the wound healing process: a literature review]. Rev Bras Pl Med 2014;16:628-36.
3. Carvalho ACB, Silveira,D. Drogas vegetais: uma antiga nova forma de utilização de plantas medicinais [Herbal drugs: an ancient new way of using medicinal plants]. Brasília Médica 2010;48:219-37.
4. Melguizo-Rodríguez L, de Luna-Bertos E, Ramos-Torrecillas J, et al. Potential effects of phenolic compounds that can be found in olive oil on wound healing. Foods 2021;10:1642.
5. Van de Velde F, Esposito D, Grace M.H, et al. Anti-inflammatory and wound healing properties of polyphenolic extracts from strawberry and blackberry fruits. Food Res Int 2019;121: 453-62.
6. Subramanian S, Duraipandian C, Alsayari A, et al. Wound healing properties of a new formulated flavonoid-rich fraction from *Dodonaea viscosa* Jacq. leaves extract. Front Pharmacol 2023;14:151.
7. Gonzalez ACDO, Andrade ZDA, Costa TF, Medrado ARAP. Wound healing-a literature review. An Bras De Dermatol 2016;91:614-20.
8. Landén N.X, Li D, Ståhle M. Transition from inflammation to

proliferation: a critical step during wound healing. Cell Mol Life Sci 2016; 73:3861-885.
9. Boyd A, Bleakley C, Gill C, et al. Herbal medicinal products or preparations for neuropathic pain and fibromyalgia. Cochrane Database Syst Rev 2013; 5:CD010528.
10. Pintore G, Usai M, Bradesi P, et al. Chemical composition and antimicrobial activity of *Rosmarinus officinalis* L. oils from Sardinia and Corsica. Flavour Fragr J 2002;17:15-9.
11. Jardak M, Elloumi-Mseddi J, Aifa S, Mnif S. Chemical composition, anti-biofilm activity and potential cytotoxic effect on cancer cells of *Rosmarinus officinalis* L. essential oil from Tunisia. Lipids Health Dis 2017;16:190.
12. Aref AR. Herbs as a food and medicine source in Palestine.Asian Pac J Cancer Prev 2005; 6:404-7.
13. De Moura FBR, Ferreira BA, Deconte SR, et al. Wound healing activity of the hydroethanolic extract of the leaves of *Maytenus ilicifolia* Mart. ex Reis. J Tradit Complement Med 2021;11:446-56.
14. Ehrlich HP, Hunt TK. The effect of cortisone and anabolic steroids on the tensile strength of healing wounds. Ann Surg 1968;57:117.
15. Collier HO, Dinneen LC, Johnson CA, Schneider C. The abdominal construction response and its suppression by analgesic drugs in the mouse. Br J Pharmacol Chemother 1986;32:295-310.
16. Waterhouse A, Bertoni M, Bienert S, et al. SWISS-MODEL: Homology modelling of protein structures and complexes. Nucleic Acids Res 2018;46:W296-W303.
17. Wiederstein M, Sippl MJ. ProSA-web: interactive web service for the recognition of errors in three-dimensional structures of proteins. Nucleic Acids Res 2007;35:W407-W10.
18. Neuberger A, Oda M, Nikolaev YA, et al. Human TRPV1 structure and inhibition by the analgesic SB-366791. Nat Commun 2023;14:2451.
19. Elyemni M, El Ouadrhiri F, Lahkimi A, et al. Chemical composition and antimicrobial activity of essential oil of wild and cultivated *Rosmarinus officinalis* from two Moroccan localities. J Ecol Eng 2022;23:214-22.
20. Andrade JM, Faustino C, Garcia C, et al. *Rosmarinus officinalis* L.: An update review of its phytochemistry and biological activity. Future Sci 2018;4:FSO283.
21. Harkat-Madouri L, Asma B, Madani K, et al. Chemical composition, antibacterial and antioxidant activities of essential oil of *Eucalyptus globulus* from Algeria. Ind Crops Prod 2015;78:148-53.
22. Barreto RS, Albuquerque-Júnior RL, Araújo AA, et al. A systematic review of the wound-healing effects of monoterpenes and iridoid derivatives. Molecules 2014;19:846-62.
23. Labib RM, Ayoub IM, Michel HE, et al. Appraisal on the wound healing potential of *Melaleuca alternifolia* and *Rosmarinus officinalis* L. Essential oil-loaded chitosan topical preparations. PLoS ONE 2019;14:e0219561.
24. Bajalan R, Rouzbahani A, Pirbalouti G, Maggi F. Quali-quantitative variation of essential oil from Iranian rosemary (*Rosmarinus officinalis* L.) accessions according to environmental factors. J Essent Oil Res 2018;30:16-24.
25. Benchohra HA, Dif MM, Ayache A. Medjaher HES. Valorization of essential oil of *Rosmarinus officinalis* L. from El Bayadh region-Algeria, Egypt. Acad J Biolog Sci 2022;14: 373-81.
26. Prabhu VV, Nalini G, Chidambaranathan N, Kisan NS. Evaluation of anti-inflammatory and analgesic activity of *Tridax procumbens* Linn against formalin, acetic acid and CFA induced pain models. Int J Pharm Pharm Sci 2011;3:126-30.
27. Zaman A, Khan MSS, Akter L, et al. Exploring new pharmacology and toxicological screening and safety evaluation of one widely used formulation of Nidrakar Bati from South Asia region. BMC Complement Altern Med 2015;15:1-22.
28. de Almeida Júnior J S, da Silva ÉBS, Moraes TMP, et al. Anti-inflammatory potential of the oleoresin from the amazonian tree *Copaifera reticulata* with an unusual chemical composition in rats. Vet Sci 2021;8:320.

Online supplementary material:

Figure 1S. Photograph of wound area after topical application of essential oil cream of S. rosmarinus *and Madecassol® cream of excision wound model in mice.*

Figure 2S. Photograph of wound area after topical application of essential oil cream of S. rosmarinus *and Madecassol® cream of incision wound model in mice.*

Figure 3S. Effect of S. rosmarinus *on acetic acid-induced writhing in mice.*

Figure 4S. Pore loop 3D modeling and validation include: (a) superposition of the modeled subunit (in green color) with one subunit of the tetrameric structure, (b) subunit of hTRPV1 with truncated pore loop (red color), (c) superposition of the two subunits of hTRPV1 with truncated pore loop and modeled pore loop, and (d) subunit of hTRPV1 with modeled loop (in green color). Validation: (e) ProSA-web, with a Z score of -7.58 for one subunit included the modeled Pore loop and Z score of -1.01 for the modeled Pore loop, as well as the local model quality by plotting energies as a function of amino acid sequence position (Pore loop region is bordered in red) (f) Ramachandran plot analysis showing in favored (dark green) and allowed (light green), regions of protein residues.

Figure 5S. Analysis of the RMSD for the (a) COX2/α-calacorene complex throughout 300ns; COX2-Cα and α-calacorene RMSD are colored in black and red respectively, (b) supported by view of superposition of 41 binding poses of the COX-2/α-calacorene complex, (ligand is shown in yellow). (c) Root Mean Square Fluctuations (RMSF) of the COX-2 Cα atoms compared with the temperature factor (B factor) for 300ns trajectory. The regions corresponding to alpha-helix and beta-sheet structures are indicated by red and blue backgrounds, respectively.

Figure 6S. Analysis of the RMSD for the (a) hTRPV1/β-bisabolene complex throughout 300ns; TRPV1-Cα and β-bisabolene RMSD are colored in blue and red respectively, (b) supported by view of superposition of 41 binding poses of the β-bisabolene complex, (ligand is shown in yellow). (c) Root mean square fluctuations (RMSF) of the TRPV1Cα atoms compared with the temperature factor (B-factor) for 300ns trajectory. The modeled Pore loop B-factor is shown in red, alpha-helix and beta-sheet regions are highlighted in red and blue backgrounds, respectively.

Table 1S. Docking binding affinity of the screened compounds against hCOX-2 and hTRPV1.